

Indirect measurement of quarkonium in the two-photon processWen-Long Sang,^{1,2} Ying-Jia Gao,³ and Yu-Qi Chen³¹*Institute of High Energy Physics, Chinese Academy of Sciences, Beijing 100049, China*²*Theoretical Physics Center for Science Facilities, Chinese Academy of Sciences, Beijing 100049, China*³*Key Laboratory of Frontiers in Theoretical Physics, Institute of Theoretical Physics, Academia Sinica, Beijing 100190, China*

(Received 7 May 2012; published 31 October 2012)

In this paper, we propose a new approach to probe the quarkonium at the BES-III and the B factories. In the two-photon process, $e^+e^- \rightarrow e^+e^- + \text{hadron}$, the signals of the emitted hadron can be reconstructed through investigating the final leptons e^+e^- . Furthermore, by analyzing the distribution of the relative angle between the final e^+ and e^- , we can determine the quantum number of the final hadron. For those hadrons that are hard to detect directly, this may provide an effective way. We calculate the cross sections as well as the distributions of the $\eta_c(1S, 2S)$ and $\chi_{cJ}(1P, 2P)$ production at tree level and the next-to-leading order QCD radiative corrections. In addition, the cross sections of bottomonium production are considered at tree level. Unfortunately, they are too tiny to be detected.

DOI: [10.1103/PhysRevD.86.074031](https://doi.org/10.1103/PhysRevD.86.074031)

PACS numbers: 12.38.-t, 12.38.Bx

I. INTRODUCTION

KEKB, PEP-II, and BEPC-II are high luminosity e^+e^- colliders running at bottom and charm quark energy scales. In these machines, the C -even quarkonium like η_c , χ_{cJ} ($J = 0, 1, 2$) and their excited states can be produced through the two-photon process, in which a quarkonium is produced via the fusion of two virtual photons emitted from an electron and a positron. The two-photon process, which is widely studied [1], is particularly useful for searching quarkonia which are hard to produce and detect via some other processes. Normally quarkonium can be measured by detecting its decay particles, however, unlike J/ψ and Υ , η_c , χ_{cJ} typically possess relatively large decay rates and small branching fractions for clean exclusive annihilation decay channels [2,3], and therefore are relatively hard to detect.

In this paper, we propose an indirect method to detect quarkonium in the two-photon process. This method is based on the following ideas: in the two-photon process, the final state's electron and positron are mainly emitted in a small azimuth angle θ away from the beam direction, however, at the B factories and BES-III, the total energies in the center of mass (c.m.) frame are not extremely high, and thus the contributions from the relative large angle are not ignorable. As a consequence, we anticipate that there are considerable electrons and positrons from the large angles recorded in the detectors. The momenta of the both virtual photons can be reconstructed from the momentum differences of the electron and positron between the initial states and the final states, and thus the momentum and the invariant mass of the produced quarkonium can be determined. The quarkonium appears as a peak in the invariant mass spectrum, from which the mass and the decay width of the quarkonium can be determined. The quantum numbers of the quarkonium can be distinguished by measuring the distribution of the relative angle between the electron and the positron.

Since the electron and positron in the final states are observed, an appropriate angular cutoff should be taken to render the emitted leptons deviating from the beam direction. Since the cross sections are small, we emphasize here that the indirect method is available only at high luminosity e^+e^- colliders such as the KEKB, PEP-II, and BEPC-II. In addition, the probable backgrounds should be separated. The two-photon process may suffer contamination from two primary backgrounds $e^+e^- \rightarrow e^+e^- \gamma$ and $e^+e^- \rightarrow e^+e^- \gamma\gamma$. As a matter of fact, events from the process $e^+e^- \rightarrow e^+e^- \gamma$ can be removed by analyzing the invariant mass spectrum of the two virtual photons, which is at origin far away from the mass of quarkonium. The other background, $e^+e^- \rightarrow e^+e^- \gamma\gamma$, the cross section of which will be estimated in this paper, can also be separated by noticing there is not a peak in the invariant mass spectrum. In this paper, we will show that a number of events via this approach can be observed at these colliders.

Compared with the conventional direct measurement, this indirect method embraces several advantages. First, the electron and positron are relatively easy to detect, hence, it is quite efficient in detecting those quarkonia with large decay rates and small branching fractions for clean exclusive decay modes. It can be used as the complementarity of the direct measurement. Second, the distribution of the azimuth angle between the emitted electron and positron can be used to determine the quantum number of the associated produced quarkonium. It can also be used to distinguish $Q\bar{Q}$ states and non- $Q\bar{Q}$ states, in particular, confirm or deny the assumptions that some of the newly discovered particles X, Y, Z are charmonium states.

The remainder of the paper is organized as follows. In Sec. II, we present the differential cross section of quarkonium production in the two-photon process within the framework of the nonrelativistic QCD (NRQCD) factorization formula. We also briefly discuss the relation between our results and the equivalent photon approximation (EPA) at

tree level. In Sec. III, we evaluate cross sections numerically at the B factories and BES-III through selecting various angle cutoffs. The cross sections for charmonium production at the BES-III are also evaluated by taking different c.m. energies. In addition, we present the distributions of the relative angle between the final e^+ and e^- for various charmonia. Section IV is devoted to the summaries and discussions.

II. CROSS SECTION OF THE TWO-PHOTON PROCESS

A. At tree level

In e^+e^- colliders, a C -even quarkonium production through the two-photon process can be described as e^+e^- splitting into $e^+e^-\gamma^*\gamma^*$, followed by formation of the quarkonium via $\gamma^*\gamma^*$ fusion, as shown in Fig. 1. The virtual photons are space-like, however, in the high-energy limit, $\sqrt{s} \gg m_e$, where \sqrt{s} and m_e are c.m. energy and the mass of electron, dominant contributions arise from the kinetic regions where almost on-shell photons are collinearly emitted from leptons. Therefore, the cross sections can be approximately evaluated in the EPA [4]. Nevertheless, at the KEKB, PEP-II, and BEPC-II, the c.m. energy \sqrt{s} is not as large as that in the LEP. As a result, there will be quite a lot of emitted electrons and positrons deviating from the beam direction that can be recorded in the detectors. Therefore, we take a complete calculation for this process instead of EPA. We first calculate the cross section at tree level, and then extend to the next-to-leading order (NLO) QCD corrections.

The quarkonium production process can be analyzed in the framework of the NRQCD factorization formula [5]. The NRQCD factorization formula for the cross section of the two-photon process is written as

$$\sigma = \frac{F_1(n)}{m^2} \langle 0 | \chi^\dagger \mathcal{K}_n \psi | H \rangle \langle H | \psi^\dagger \mathcal{K}_n \chi | 0 \rangle + \mathcal{O}(v^2 \sigma), \quad (1)$$

where m denotes the mass of the heavy quark in the quarkonium H , \mathcal{K}_n signify

$$\begin{aligned} \mathcal{K}_{1S_0} &= 1, & \mathcal{K}_{3P_0} &= \frac{1}{\sqrt{3}} \left(-\frac{i}{2} \vec{D} \cdot \sigma \right), \\ \mathcal{K}_{3P_1} &= \frac{1}{\sqrt{2}} \left(-\frac{i}{2} \vec{D} \times \sigma \right) \cdot \epsilon_H, & & \\ \mathcal{K}_{3P_2} &= -\frac{i}{2} \vec{D}^{(i} \sigma^{j)} \epsilon_H^{ij}, & & \end{aligned} \quad (2)$$

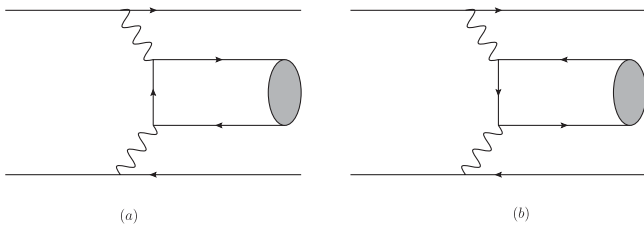


FIG. 1. Feynman diagrams for $e^-(k_1)e^+(k_2) \rightarrow e^-(k'_1)e^+(k'_2) + H$ at tree level.

and $F_1(n)$ are the short-distance coefficients corresponding to the matrix elements. In (1), we have neglected the high-order relativistic correction terms. Generally, the short-distance coefficients can be expanded in powers of α_s at energy scales of m or higher. Since the short-distance coefficients are insensitive to the nonperturbative effects, they can be determined by matching the cross sections of the two-photon process with the quarkonia substituted by free heavy-quark pairs possessing the same quantum numbers as the quarkonia in the full QCD to those in the NRQCD.

To this end, we first calculate the cross section of the process $e^+(k_1)e^-(k_2) \rightarrow e^+(k'_1)e^-(k'_2)Q(p_1)\bar{Q}(p_2)$ with the $Q(p_1)\bar{Q}(p_2)$ pair near threshold in the QCD. At tree level, the Feynman diagrams are shown in Fig. 1. We assign P and q as the total and half relative momenta of the $Q\bar{Q}$ pair, immediately there are

$$\begin{aligned} p_1 &= \frac{1}{2}P + q, & p_2 &= \frac{1}{2}P - q, \\ p_1^2 &= p_2^2 = m^2, & P \cdot q &= 0. \end{aligned} \quad (3)$$

At tree level, the amplitude \mathcal{M} of this process is expressed as

$$\begin{aligned} \mathcal{M}_{e^+e^- \rightarrow e^+e^-Q\bar{Q}} &= e_Q^2 e^2 \bar{u}(k'_1) \gamma_\mu u(k_1) \frac{1}{\ell_1^2} \bar{v}(k_2) \gamma_\nu v(k'_2) \frac{1}{\ell_2^2} \mathcal{A}_{\gamma^*\gamma^* \rightarrow c\bar{c}}^{\mu\nu}, \quad (4) \end{aligned}$$

where e_Q is the electric charge of the heavy quark and $\mathcal{A}_{\gamma^*\gamma^* \rightarrow Q\bar{Q}}^{\mu\nu}$ denotes the amplitude of the process $\gamma^*(\ell_1)\gamma^*(\ell_2) \rightarrow Q(p_1)\bar{Q}(p_2)$:

$$\begin{aligned} \mathcal{A}_{\gamma^*\gamma^* \rightarrow Q\bar{Q}}^{\mu\nu} &= e^2 \left[\frac{\gamma^\mu (\not{p}_1 - \not{\ell}_1 + m) \gamma^\nu}{\ell_1^2 - 2p_1 \cdot \ell_1} \right. \\ &\quad \left. + \frac{\gamma^\nu (\not{p}_1 - \not{\ell}_2 + m) \gamma^\mu}{\ell_2^2 - 2p_1 \cdot \ell_2} \right]. \quad (5) \end{aligned}$$

Momentum conservation implies that $\ell_1 = k_1 - k'_1$ and $\ell_2 = k_2 - k'_2$.

To impose the quantum number of $^1S_0, ^3P_J$ on the free quark pair, we employ the spin projector operator Π_m , where for the spin-singlet state, Π_0 reads [6]

$$\Pi_0 = \frac{(\not{P}/2 - \not{q} - m) \gamma_5 (\not{P}/2 + \not{q} + m)}{4\sqrt{2N_c} E(E+m)}, \quad (6)$$

and for the spin-triplet state with spin-polarization vector ϵ , Π_1 reads [6]

$$\Pi_1 = -\frac{(\not{P}/2 - \not{q} - m) \epsilon^* (\not{P}/2 + \not{q} + m)}{4\sqrt{2N_c} E(E+m)}, \quad (7)$$

where $E = \sqrt{m^2 + \mathbf{q}^2}$. In the leading order at velocity expansion, we are allowed to take $E = m$.

Multiplying $\mathcal{A}^{\mu\nu}$ with the projector operator Π_m and taking the trace of the product, we obtain the amplitude for $Q\bar{Q}(\text{spin} = m)$ production:

$$\tilde{\mathcal{A}}^{\mu\nu} = \text{Tr}[\mathcal{A}^{\mu\nu}\Pi_m]. \quad (8)$$

Furthermore, we need to extract the correct orbital and total angular momentum for the free quark pair. For 1S_0 , the operation is trivial, and we only need to put the relative momentum to zero, while for 3P_J , we employ the formulas [7,8]:

$$\tilde{\mathcal{A}}^{\alpha\beta}(\lambda_H) = |\mathbf{q}| \frac{\partial}{\partial q^\mu} \text{Tr}[\mathcal{A}^{\alpha\beta}\Pi_{1\nu}]\mathcal{P}_J^{\mu\nu}, \quad (9)$$

where Π_1^ν is defined via $\Pi_1 \equiv \Pi_1^\nu \epsilon^\nu$ and the projection operators $\mathcal{P}_J^{\mu\nu}$ are defined by

$$\begin{aligned} \mathcal{P}_0^{\mu\nu} &= \frac{1}{\sqrt{3}} \left(-g^{\mu\nu} + \frac{P^\mu P^\nu}{4E^2} \right), \\ \mathcal{P}_1^{\mu\nu} &= \frac{i}{2\sqrt{2}E} \epsilon^{\mu\nu\rho\sigma} P_\rho \epsilon_{\lambda_H\sigma}^*, \\ \mathcal{P}_2^{\mu\nu} &= \epsilon_{\lambda_H}^{*\mu\nu}. \end{aligned} \quad (10)$$

With these techniques, we are able to obtain the amplitudes for $Q\bar{Q}(^1S_0, ^3P_J)$ production in the two-photon process. After taking the spin sum for the final states and spin average over the initial states, we obtain the unpolarized squared amplitudes. The calculation is tedious but quite straightforward, therefore, we will not give the cumbersome analytic results. In our calculation, we take the mass of the electron $m_e = 0$ from the beginning. This seems to bring singularities into the two-photon process, however, we stress that this will not happen, since we will take cutoffs for the azimuth angles between the emitted and initial leptons to make them measurable and the cutoffs will eliminate the singularities stemming from the nearly on-shell propagators of the intermediate photons.

Now, we proceed to deal with the phase-space integral, which is a three-body integral. For convenience, we choose the direction of the initial electron's momentum as z axis, and take the final electron's momentum to lie on the x - z plane. Then after making use of the momentum conservation, we remain with four independent parameters, k_1^0 (the energy of the final electron), θ (the angle between the initial and final electron), η (the angle between the initial and final positron), and ϕ (the angle between the projections of 3-momenta of the final e^+ and e^- on the x - y plane).

Thus, the phase-space integral reduces to

$$\begin{aligned} d\Gamma(2 \rightarrow 3) &= \frac{1}{2s} \int \frac{d^3\vec{k}'_1}{(2\pi)^3 2E_1} \frac{d^3\vec{k}'_2}{(2\pi)^3 2E_2} \frac{d^4P}{(2\pi)^3} \delta(P^2 - M_H^2) \\ &\quad \times (2\pi)^4 \delta^{(4)}(k_1 + k_2 - k'_1 - k'_2 - P) \\ &= \frac{1}{2s} \frac{1}{4(2\pi)^4} \int dk_1^0 dk_2^0 d\cos\theta d\cos\eta d\phi \\ &\quad \times (|\vec{k}'_1| |\vec{k}'_2|) \delta(F(k_2^0)), \end{aligned} \quad (11)$$

where in the second step we have used the momentum conservation to reexpress $\delta(P^2 - M_H^2)$ as the function of k_2^0 . Finally, the cross sections are formally written as

$$\sigma^{(2S+1)L_J}_{\text{QCD}} = \int d\Gamma \frac{1}{4} \sum_{\text{pol}} |\mathcal{M}^{(2S+1)L_J}|^2, \quad (12)$$

where $\mathcal{M}^{(2S+1)L_J}$ are the production amplitude of the process $e^+e^- \rightarrow e^+e^-Q\bar{Q}(^{2S+1}L_J)$.

Though the squared amplitudes are cumbersome, it is interesting as well as enlightening to take the limit: $\cos\theta \rightarrow 1$, $\cos\eta \rightarrow 1$, which corresponds to the emitted electron (positron) collinear with the initial electron (positron). The squared amplitudes in this limit yield

$$\begin{aligned} \frac{1}{4} \sum_{\text{pol}} |\mathcal{M}(^1S_0)|^2 &= \frac{1024N_c\pi^4 e_Q^4 \alpha^4 [(y_1^2 + 1)r^2 + 2(y_1 - 1)(y_1 + 1)^2 r + 2(y_1^2 - 1)^2]}{m^4(y_1 - 1)y_1(r + y_1 - 1)(1 - \cos\theta)(1 - \cos\eta)} - \frac{8192N_c\pi^4 e_Q^4 \alpha^4 \cos^2\phi}{m^4(1 - \cos\theta)(1 - \cos\eta)}, \\ \frac{1}{4} \sum_{\text{pol}} |\mathcal{M}(^3P_0)|^2 &= \frac{3072N_c\pi^4 e_Q^4 \alpha^4 |\mathbf{q}|^2 [2(y_1 - 1)^4 + 2r(y_1 - 1)^3 + r^2(y_1^2 + 1)]}{m^6(y_1 - 1)y_1(r + y_1 - 1)(1 - \cos\theta)(1 - \cos\eta)} + \frac{24576N_c\pi^4 e_Q^4 \alpha^4 |\mathbf{q}|^2 \cos^2\phi}{m^6(1 - \cos\theta)(1 - \cos\eta)}, \\ \frac{1}{4} \sum_{\text{pol}} |\mathcal{M}(^3P_1)|^2 &= 0, \\ \frac{1}{4} \sum_{\text{pol}} |\mathcal{M}(^3P_2)|^2 &= \frac{4096N_c\pi^4 e_Q^4 \alpha^4 |\mathbf{q}|^2 [r^2 + 2(y_1 - 1)r + 2(y_1 - 1)^2](y_1^2 + 1)\alpha^4}{m^6(y_1 - 1)y_1(r + y_1 - 1)(1 - \cos\theta)(1 - \cos\eta)}, \end{aligned} \quad (13)$$

where $r \equiv \frac{4m^2}{s}$, $y_1(y_2) = \frac{2k_1^0}{\sqrt{s}} (\frac{2k_2^0}{\sqrt{s}})$ denote the energy fractions of the emitted electron (positron), and the sum runs over all the polarizations of both the initial and final states. Furthermore, averaging over the relative angle ϕ in (13), we obtain

$$\int \frac{d\phi}{2\pi} \frac{1}{4} \sum_{\text{pol}} |\mathcal{M}(H)|^2 = \mathcal{N}_H \frac{16\pi^2 [r^2 + 2(y_1 - 1)r + 2(y_1 - 1)^2](y_1^2 + 1)\alpha^2}{m^4(y_1 - 1)y_1(r + y_1 - 1)(1 - \cos\theta)(1 - \cos\eta)}, \quad (14)$$

where for H to be 1S_0 , 3P_0 , 3P_1 , and 3P_2 , \mathcal{N}_H are $64N_c\pi^2 e_Q^2 \alpha^2$, $192N_c\pi^2 e_Q^2 \alpha^2/m^2$, 0, and $256N_c\pi^2 e_Q^2 \alpha^2/m^2$, respectively.

Actually, (14) is nothing but the results from EPA. To see this, one can derive the squared amplitudes from the EPA directly. The squared amplitudes of the electron and positron splitting processes read [9]

$$\begin{aligned} \frac{1}{2} \sum_{\text{pol}} |\mathcal{M}(e^+ \rightarrow e^+ \gamma)|^2 &= \frac{8m^2 \pi y_1 (y_1^2 + 1) \alpha \sin^2 \theta}{r(y_1 - 1)^2} \times \left(\frac{1}{\ell_1^2}\right)^2, \\ \frac{1}{2} \sum_{\text{pol}} |\mathcal{M}(e^- \rightarrow e^- \gamma)|^2 &= \frac{8m^2 \pi y_2 (y_2^2 + 1) \alpha \sin^2 \eta}{r(y_2 - 1)^2} \times \left(\frac{1}{\ell_2^2}\right)^2, \end{aligned} \quad (15)$$

where the propagators of the immediate states photons have been included in (15). Meanwhile the squared amplitudes of the two-photon fusion processes read

$$\begin{aligned} \frac{1}{4} \sum_{\text{pol}} |\mathcal{M}(\gamma\gamma \rightarrow {}^1S_0)|^2 &= 64N_c \pi^2 e_Q^4 \alpha^2, \\ \frac{1}{4} \sum_{\text{pol}} |\mathcal{M}(\gamma\gamma \rightarrow {}^3P_0)|^2 &= \frac{192N_c \pi^2 e_Q^4 \alpha^2 |\mathbf{q}|^2}{m^2}, \\ \frac{1}{4} \sum_{\text{pol}} |\mathcal{M}(\gamma\gamma \rightarrow {}^3P_1)|^2 &= 0, \\ \frac{1}{4} \sum_{\text{pol}} |\mathcal{M}(\gamma\gamma \rightarrow {}^3P_2)|^2 &= \frac{256\pi^2 \alpha^2 |\mathbf{q}|^2}{m^2}. \end{aligned} \quad (16)$$

Multiplying (15) with (16), using the energy conservation to swap y_2 for y_1 ($y_2 = \frac{1-r-y_1}{1-y_1}$), we readily reach the formula (14).

Next, we turn to evaluate the cross sections of the same processes in the NRQCD factorization formula. Since the calculation is simple and direct, we present the final results

$$\begin{aligned} \sigma({}^1S_0)_{\text{NRQCD}}^{(0)} &= 8N_c F^{(0)}({}^1S_0), \\ \sigma({}^3P_J)_{\text{NRQCD}}^{(0)} &= 8N_c F^{(0)}({}^3P_J) |\mathbf{q}|^2, \end{aligned} \quad (17)$$

where the superscript (0) denotes the quantity at tree level. $F({}^1S_0)$ and $F({}^3P_J)$ are the short-distance coefficients of the cross sections for η_Q production and χ_{QJ} production, respectively.

Through matching the cross sections of $e^+e^- \rightarrow e^+e^- Q\bar{Q}({}^1S_0, {}^3P_J)$ in the full QCD to those in the NRQCD, we can obtain the short-distance coefficients immediately. Finally, the cross sections for the η_Q and χ_{QJ} production in the two-photon process are expressed as

$$\begin{aligned} \sigma(\eta_Q)^{(0)} &= \sigma({}^1S_0)_{\text{QCD}}^{(0)} \frac{\langle 0 | \chi^\dagger \psi | \eta_c \rangle \langle \eta_c | \psi^\dagger \chi | 0 \rangle}{8N_c m^2} \\ &= \sigma({}^1S_0)_{\text{QCD}}^{(0)} \frac{\langle 0 | \chi^\dagger \psi | \eta_c \rangle \langle \eta_c | \psi^\dagger \chi | 0 \rangle_{\text{BBL}}}{2N_c m}, \\ \sigma(\chi_{QJ})^{(0)} &= \sigma({}^3P_J)_{\text{QCD}}^{(0)} \frac{\langle 0 | \chi^\dagger \mathcal{K}_J \psi | \chi_J \rangle \langle \chi_J | \psi^\dagger \mathcal{K}_J \chi | 0 \rangle}{8N_c m^2 |\mathbf{q}|^2} \\ &= \sigma({}^3P_J)_{\text{QCD}}^{(0)} \frac{\langle 0 | \chi^\dagger \mathcal{K}_J \psi | \chi_J \rangle \langle \chi_J | \psi^\dagger \mathcal{K}_J \chi | 0 \rangle_{\text{BBL}}}{2N_c m |\mathbf{q}|^2}, \end{aligned} \quad (18)$$

where we employed the relations [10]

$$\langle 0 | \chi^\dagger \mathcal{K}_n \psi | H \rangle = \sqrt{4m} \langle 0 | \chi^\dagger \mathcal{K}_n \psi | H \rangle_{\text{BBL}} + \mathcal{O}(v^2). \quad (19)$$

In above equation, the hadron state on the left-hand side is normalized relativistically, while is normalized nonrelativistically on the right-hand side.

B. NLO radiative corrections

For charmonium production, the strong coupling constant at the scales of the charm quark mass is moderate ($\alpha_s(2m_c) = 0.26$), therefore, the NLO radiative corrections may bring considerable contributions. Moreover, some recent works [11,12] reveal that the NLO radiative corrections to the cross sections of $e^+e^- \rightarrow H\gamma$ are not negligible. Especially for χ_{c2} production, the NLO radiative corrections modify the tree-level result by a huge margin. Motivated by these reasons, we will calculate the NLO radiative corrections to quarkonium production in the two-photon process.

Following the same strategy as in the previous section, we apply the method of matching to obtain the short-distance coefficients, and then obtain the cross sections. We first calculate the cross sections of $e^+e^- \rightarrow e^+e^- c\bar{c}({}^1S_0, {}^3P_J)$ in the QCD. The Feynman diagrams in one loop are illustrated in Fig. 2, which include two self-energy diagrams, four triangle diagrams, and two box diagrams. We perform the renormalization in on-mass-shell scheme and take dimensional regularization to regulate both the ultraviolet (UV) and the infrared (IR) divergences. In the on-mass-shell scheme, external quark lines do not receive any QCD corrections, and the counterterms from the renormalization constants of the heavy quark wave function and the heavy quark mass are given by

$$\begin{aligned} \delta Z_Q^{\text{OS}} &= -C_F \frac{\alpha_s}{4\pi} \left(\frac{1}{\epsilon_{\text{UV}}} + \frac{2}{\epsilon_{\text{IR}}} - 3\gamma_E + 3 \ln \frac{4\pi\mu^2}{m_c^2} + 4 \right) \\ &\quad + \mathcal{O}(\alpha_s^2), \end{aligned} \quad (20)$$

$$\delta Z_{m_Q}^{\text{OS}} = -C_F \frac{\alpha_s}{4\pi} \left(\frac{3}{\epsilon_{\text{UV}}} - 3\gamma_E + 3 \ln \frac{4\pi\mu^2}{m_c^2} + 4 \right) + \mathcal{O}(\alpha_s^2), \quad (21)$$

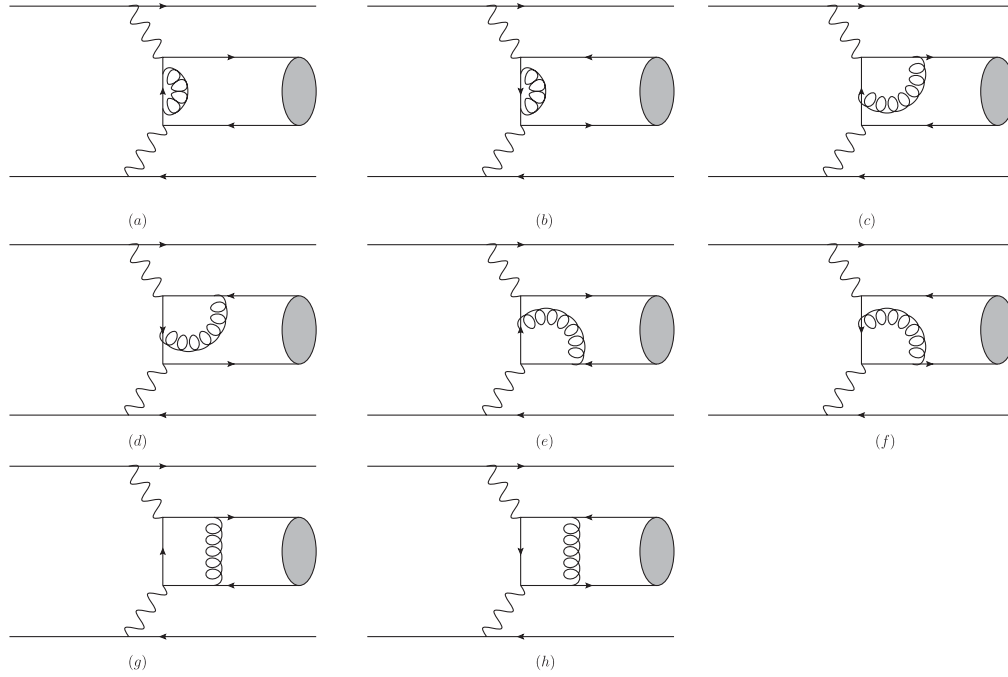


FIG. 2. The Feynman diagrams for the two-photon process in one loop.

where μ is the renormalization scale, γ_E is the Euler's constant, and $C_F = \frac{4}{3}$ for $SU(3)_c$.

The divergences of the diagrams in Fig. 2 can be analyzed as follows: the self-energy and the triangle diagrams contain UV divergences, while the box diagrams possess IR divergences. In addition, Coulomb singularities may arise from the box diagrams, due to the exchange of the longitudinal gluon between c and \bar{c} . Our calculation indicates that the UV divergences from the self-energy and the triangle diagrams are canceled by those from the renormalization constants of the quark field and the mass, and the IR divergences from the box diagrams are canceled by those in δZ_Q . Finally, the remaining Coulomb singularities will be canceled by the Coulomb singularities in the NRQCD matrix elements by the matching condition. In our practical calculation, the FEYNCALC package [13] has been employed to take the trace of the γ -matrix and to reduce tensor integrals into scalar ones. To check the validity of our results, we make several cross-checks to the subprocess $\gamma^* \gamma^* \rightarrow c\bar{c}(^1S_0, ^3P_J)$: first, the amplitudes satisfy the Ward-Identity for both virtual photons; second, in the limit $\ell_1^2 = \ell_2^2 = 0$, the squared amplitudes by summing the polarizations of the two photons reduce to those of $c\bar{c}(^1S_0, ^3P_J) \rightarrow \gamma\gamma$; third, when we take the limit $\ell_1^2 = 0$, $\ell_2^2 = s > 4m_c^2$ for the momenta of the two photons, the squared amplitudes reduce to the analytical expressions in Ref. [11].

The analytical expressions are intricate and cumbersome, so we will not give them in this paper. The calculation in the NRQCD factorization formula is quite straightforward:

$$\sigma(^1S_0)_{\text{NRQCD}} = 8N_c F(^1S_0) \left(1 + \frac{\pi^2}{v} C_F \frac{\alpha_s}{\pi} \right), \quad (22)$$

$$\sigma(^3P_J)_{\text{NRQCD}} = 8N_c F(^3P_J) |\mathbf{q}|^2 \left(1 + \frac{\pi^2}{v} C_F \frac{\alpha_s}{\pi} \right),$$

where the Coulomb singularities are exactly canceled by those in the QCD. Finally, we are able to get the short-distance coefficients $F(^1S_0, ^3P_J)$ and readily the cross sections of the two-photon process in the NLO in α_s .

III. NUMERICAL RESULTS

In the following, we apply the formulas derived in the last section to numerically evaluate the cross sections. The relevant input parameters must be selected. We choose the c.m. energies to be $\sqrt{s} = 10.6$ GeV at the KEKB and PEP-II, and $\sqrt{s} = 3.78$ GeV at the BEPC-II. In addition, several different c.m. energies ranging from 4.0 to 6.0 GeV are taken at the BEPC-II to make predictions; the fine structure constant and strong coupling constant are taken as $\alpha = 1/131$ and $\alpha_s(2m_c) = 0.26$; charm and bottom quark pole masses are taken as $m_c = 1.4$ GeV and $m_b = 4.6$ GeV, respectively; the mass of the electron is neglected as mentioned in the previous section; the masses of the hadrons are taken as [3]

$$\begin{aligned} m_{\eta_c} &= 2.980 \text{ GeV}, & m_{\eta_c(2S)} &= 3.637 \text{ GeV}, \\ m_{\chi_{c0}} &= 3.415 \text{ GeV}, & m_{\chi_{c1}} &= 3.511 \text{ GeV}, \\ m_{\chi_{c2}} &= 3.556 \text{ GeV}, & m_{\chi_{c2(2P)}} &= 3.929 \text{ GeV}, \\ m_{\eta_b} &= 9.392 \text{ GeV}, & m_{\chi_{b0}} &= 9.859 \text{ GeV}, \\ m_{\chi_{b1}} &= 9.892 \text{ GeV}, & m_{\chi_{b2}} &= 9.912 \text{ GeV}. \end{aligned} \quad (23)$$

TABLE I. The cross sections (in units of fb) for charmonium and bottomonium production. The azimuth angle cutoffs for the electron and positron are chosen to be $\theta_{\text{cut}} = \eta_{\text{cut}} = 20^\circ$ in the laboratory reference frame.

	η_c	$\eta_c(2S)$	χ_{c0}	χ_{c1}	χ_{c2}	η_b	χ_{b0}	χ_{b1}	χ_{b2}
BES-III	102.4	4.8	3.0	0.01	2.5				
Belle	75.3	24.1	2.6	2.5	4.2	0.06	0.005	0.00002	0.003
BABAR	68.0	21.9	2.4	2.2	3.7	0.06	0.005	0.00002	0.003

We take the masses of $\chi_{c0}(2P)$, $\chi_{c1}(2P)$ as $m_{\chi_{c0}(2P)} = 3.932$ GeV, $m_{\chi_{c1}(2P)} = 4.008$ GeV [14], which are calculated from the Cornell potential. Since we will not consider the relativistic corrections, it is consistent to take the masses of the quarkonia as $2m$ through the whole calculation, however, there is a subtlety here, the phase-space integral is sensitive to the masses of the hadrons for charmonium production at the BES-III and bottomonium production at the B factories. As a result, it is more rational to use the physical masses of hadrons other than $2m$, which corresponds to resum a group of relativistic corrections from the phase-space integral [15]. To maintain gauge invariance, we should also put the masses of the heavy quark to $m = M_H/2$ in the amplitudes so as to respect the on-shell condition [15]. This replacement is available in the leading order in v^2 [5].

The NRQCD matrix elements are also required [16–20]:

$$\begin{aligned}
\langle 0 | \chi^\dagger \psi | \eta_c \rangle \langle \eta_c | \psi^\dagger \chi | 0 \rangle &= 0.398 \text{ GeV}^3, \\
\langle 0 | \chi^\dagger \psi | \eta_c(2S) \rangle \langle \eta_c(2S) | \psi^\dagger \chi | 0 \rangle &= 0.202 \text{ GeV}^3, \\
\frac{1}{3} |\langle \chi_{c0} | \psi^\dagger \left(-\frac{i}{2} \mathbf{D} \cdot \sigma \right) \chi | 0 \rangle|^2 &= 0.051 \text{ GeV}^5 \\
\frac{1}{2} \left| \langle \chi_{c1} | \psi^\dagger \left(-\frac{i}{2} \mathbf{D} \times \sigma \cdot \epsilon_H \right) \chi | 0 \rangle \right|^2 &= 0.060 \text{ GeV}^5, \\
\left| \sum_{ij} \langle \chi_{c2} | \psi^\dagger \left(-\frac{i}{2} D^{(i} \sigma^{j)} \epsilon_H^{ij} \right) \chi | 0 \rangle \right|^2 &= 0.068 \text{ GeV}^5, \\
\langle 0 | \chi^\dagger \psi | \eta_b \rangle \langle \eta_b | \psi^\dagger \chi | 0 \rangle &= 3.07 \text{ GeV}^3, \\
\frac{1}{3} \left| \langle \chi_{b0} | \psi^\dagger \left(-\frac{i}{2} \mathbf{D} \cdot \sigma \right) \chi | 0 \rangle \right|^2 &= 2.03 \text{ GeV}^5 \\
\frac{1}{2} \left| \langle \chi_{b1} | \psi^\dagger \left(-\frac{i}{2} \mathbf{D} \times \sigma \cdot \epsilon_H \right) \chi | 0 \rangle \right|^2 &= 2.03 \text{ GeV}^5, \\
\left| \sum_{ij} \langle \chi_{b2} | \psi^\dagger \left(-\frac{i}{2} D^{(i} \sigma^{j)} \epsilon_H^{ij} \right) \chi | 0 \rangle \right|^2 &= 2.03 \text{ GeV}^5, \quad (24)
\end{aligned}$$

and for the NRQCD matrix elements of $\chi_{cJ}(2P)$, we apply the formulas $\frac{1}{3} |\langle \chi_{c0} | \psi^\dagger \left(-\frac{i}{2} \mathbf{D} \cdot \sigma \right) \chi | 0 \rangle|^2 = \frac{1}{2} |\langle \chi_{c1} | \psi^\dagger \times \left(-\frac{i}{2} \mathbf{D} \times \sigma \cdot \epsilon_H \right) \chi | 0 \rangle|^2 = |\sum_{ij} \langle \chi_{c2} | \psi^\dagger \left(-\frac{i}{2} D^{(i} \sigma^{j)} \epsilon_H^{ij} \right) \times$

TABLE II. The cross sections (in units of fb) for charmonium production. The first column corresponds to the azimuth angle cutoffs $\theta_{\text{cut}} (= \eta_{\text{cut}})$ for the electron and positron in the laboratory reference frame, and we have considered angular transformation for the cutoffs from the laboratory reference frame to the c.m. frame at the KEKB and PEP-II. The values in the same lines with ‘‘NLO’’ (red) denote the cross sections by including the tree-level results and the NLO radiative corrections. The c.m. energies are taken as $\sqrt{s} = 10.6$ GeV at the KEKB and PEP-II, and $\sqrt{s} = 3.78$ GeV at the BEPC-II.

	BES-III					Belle					BABAR				
	η_c	$\eta_c(2S)$	χ_{c0}	χ_{c1}	χ_{c2}	η_c	$\eta_c(2S)$	χ_{c0}	χ_{c1}	χ_{c2}	η_c	$\eta_c(2S)$	χ_{c0}	χ_{c1}	χ_{c2}
5°	396.7	16.1	10.8	0.03	8.6	1149.3	267.2	53.1	13.9	73.1	1104.8	258.6	50.8	13.8	70.2
NLO	286.9	11.6	11.0	0.03	4.7	831.3	193.5	54.0	11.7	38.3	799.1	187.0	51.7	11.6	36.7
7.5°	290.0	12.2	8.0	0.02	6.4	641.6	159.4	28.4	10.2	40.2	606.4	152.2	26.7	10.0	37.9
NLO	209.7	8.8	8.1	0.02	3.5	463.9	115.4	28.9	8.5	20.6	438.9	110.3	27.2	8.4	19.3
10°	224.6	9.7	6.3	0.02	5.1	386.8	102.2	16.4	7.6	23.8	360.2	96.3	15.1	7.3	22.1
NLO	162.4	7.0	6.4	0.02	2.8	279.4	74.0	16.7	6.3	11.9	260.4	69.5	15.4	6.1	11.0
12.5°	179.8	8.0	5.1	0.02	4.1	244.9	68.4	9.9	5.7	14.7	225.3	63.7	9.0	5.4	13.5
NLO	130.0	5.8	5.2	0.02	2.2	176.5	49.5	10.0	4.8	7.1	162.5	46.2	9.1	4.5	6.6
15°	147.0	6.7	4.2	0.02	3.4	160.8	47.2	6.2	4.3	9.4	146.6	43.6	5.6	4.0	8.5
NLO	106.3	4.8	4.3	0.02	1.8	115.6	34.1	6.3	3.6	4.5	105.7	31.4	5.7	3.3	4.0
17.5°	122.1	5.7	3.5	0.01	2.9	108.7	33.4	4.0	3.2	6.2	98.5	30.6	3.6	2.9	5.6
NLO	88.3	4.1	3.6	0.01	1.6	77.9	24.1	4.0	2.7	2.9	70.8	21.8	3.6	2.4	2.7
20°	102.4	4.8	3.0	0.01	2.5	75.3	24.1	2.6	2.5	4.2	68.0	21.9	2.4	2.2	3.7
NLO	74.2	3.5	3.0	0.01	1.4	53.8	17.4	2.6	2.1	1.9	48.7	15.6	2.4	1.8	1.7
22.5°	86.6	4.2	2.6	0.01	2.1	53.3	17.6	1.8	1.9	2.9	48.1	16.0	1.6	1.7	2.6
NLO	62.7	3.0	2.6	0.01	1.1	37.9	12.6	1.8	1.6	1.3	34.5	11.6	1.6	1.4	1.2
25°	73.6	3.6	2.2	0.01	1.8	38.5	13.1	1.2	1.4	2.0	34.8	11.9	1.1	1.3	1.8
NLO	53.3	2.6	2.2	0.01	1.0	27.3	9.4	1.2	1.1	0.9	24.8	8.5	1.1	1.1	0.8
27.5°	62.9	3.2	1.9	0.01	1.6	28.2	9.9	0.9	1.1	1.4	25.6	9.0	0.8	1.0	1.3
NLO	45.5	2.3	1.9	0.01	0.9	19.9	7.1	0.9	0.9	0.6	18.3	6.6	0.8	0.8	0.6
30°	53.9	2.8	1.6	0.01	1.4	21.0	7.5	0.6	0.9	1.0	19.1	6.9	0.6	0.8	0.9
NLO	39.0	2.0	1.6	0.01	0.8	14.8	5.4	0.6	0.7	0.4	13.3	5.0	0.6	0.7	0.4

TABLE III. The cross sections (in units of fb) for the $\chi_{cJ}(2P)$ production. The first column corresponds to the azimuth angle cutoff $\theta_{\text{cut}} (= \eta_{\text{cut}})$ for the electron and positron in the laboratory reference frame, and we have considered angular transformation for the cutoffs from the laboratory reference frame to the c.m. frame at the KEKB and PEP-II. The values in the same columns with ‘‘NLO’’ (red) denote the results by including the tree-level results and NLO radiative corrections.

	Belle						BABAR					
	$\chi_{c0}(2P)$		$\chi_{c1}(2P)$		$\chi_{c2}(2P)$		$\chi_{c0}(2P)$		$\chi_{c1}(2P)$		$\chi_{c2}(2P)$	
	LO	NLO										
5°	73.2	74.5	14.6	12.3	100.3	52.9	70.6	71.9	14.5	12.2	96.7	50.9
7.5°	41.6	42.3	11.1	9.3	57.4	29.7	39.4	40.1	10.9	9.1	54.4	28.0
10°	25.3	25.7	8.6	7.2	35.2	17.8	23.7	24.1	8.3	6.9	32.9	16.6
12.5°	16.1	16.4	6.7	5.6	22.5	11.1	14.9	15.2	6.3	5.3	20.8	10.3
15°	10.6	10.8	5.2	4.3	14.9	7.2	9.7	9.9	4.9	4.1	13.5	6.5
17.5°	7.1	7.2	4.1	3.4	10.0	4.7	6.5	6.6	3.7	3.1	9.1	4.3
20°	4.9	5.0	3.2	2.7	6.9	3.2	4.4	4.5	2.9	2.4	6.2	2.9
22.5°	3.4	4.4	2.5	2.1	4.9	2.3	3.1	3.1	2.2	1.8	4.4	2.0
25°	2.4	2.4	2.0	1.7	3.5	1.6	2.2	2.2	1.8	1.5	3.1	1.4
27.5°	1.8	1.8	1.6	1.3	2.5	1.1	1.6	1.6	1.4	1.2	2.2	0.9
30°	1.3	1.3	1.2	1.0	1.8	0.7	1.2	1.2	1.1	0.9	1.7	0.8

$\chi|0\rangle|^2 = \frac{3N_c}{2\pi} |R'(0)|^2 = 0.188 \text{ GeV}^5$, where the wave function at origin is employed from Ref. [21].

Finally, we must choose the cutoffs for the azimuth angles θ , η of the emitted electron and positron, which depend on the detectors. To observe the variance of the cross sections with the azimuth angles and facilitate the measurement from experiments, here, we will take $\theta_{\text{cut}} = \eta_{\text{cut}} = 5^\circ, 7.5^\circ, 10^\circ, 12.5^\circ, 15^\circ, 17.5^\circ, 20^\circ, 22.5^\circ, 25^\circ, 27.5^\circ, 30^\circ$ in the laboratory reference frame to separately evaluate the cross sections. Since the cross sections (18) are obtained in the c.m. frame, the cutoffs of the azimuth angles should be transformed from the laboratory reference frame to the c.m. frame at the KEKB ($E_{e^+} = 3.5 \text{ GeV}$, $E_{e^-} = 8 \text{ GeV}$) and at the PEP-II ($E_{e^+} = 3.1 \text{ GeV}$, $E_{e^-} = 9.0 \text{ GeV}$).

As shown in Table I, the cutoffs are taken as 20° and the cross sections of both the charmonia and the bottomonia at

tree level are listed for comparison. From the table, it is manifest that the cross sections for bottomonium production are too tiny to be detected. The reasons will be analyzed in the final section. In Tables II and III, we show the cross sections for charmonium production by taking various cutoffs of the azimuth angles in the three detectors. In the tables, the results from the same rows with the cutoffs correspond to the cross sections at tree level, while these from the same rows with the ‘‘NLO’’ correspond to the cross sections by including the NLO radiative corrections. Since the cross sections for bottomonium production are too small, they are not listed in the two tables. We also give the cross sections for charmonium production at the BES-III with several different c.m. energies ($\sqrt{s} = 4.0\text{--}6.0 \text{ GeV}$) in Table IV, where the NLO radiative corrections have been included in the cross sections.

TABLE IV. The cross sections (in units of fb) for charmonium production with various c.m. energies at the BEPC-II. The first column corresponds to the colliding energy (GeV), while the first row corresponds to the azimuth angle cutoffs $\theta_{\text{cut}} (= \eta_{\text{cut}})$ for the electron and positron in the laboratory reference frame. The NLO radiative corrections have been included in the cross sections. The η'_c, χ'_{cJ} stand for $\eta_c(2S), \chi_{cJ}(2P)$, respectively.

\sqrt{s}	15°								20°							
	η_c	η'_c	χ_{c0}	χ_{c1}	χ_{c2}	χ'_{c0}	χ'_{c1}	χ'_{c2}	η_c	η'_c	χ_{c0}	χ_{c1}	χ_{c2}	χ'_{c0}	χ'_{c1}	χ'_{c2}
4.0	124.7	11.2	6.1	0.07	3.3	1.1	...	0.8	85.6	8.3	4.3	0.05	2.3	0.8	...	0.6
4.2	138.6	16.1	7.3	0.2	4.2	3.9	0.01	2.9	93.8	11.6	5.1	0.1	2.9	2.8	0	2.0
4.4	150.7	20.6	8.4	0.3	4.9	6.3	0.03	4.5	100.4	14.6	5.7	0.3	3.4	4.5	0.03	3.1
4.6	160.5	24.3	9.3	0.4	5.5	8.1	0.1	5.7	105.7	17.0	6.1	0.3	3.7	5.7	0.1	4.0
4.8	168.9	27.3	10.0	0.6	6.0	9.7	0.2	6.8	109.8	18.9	6.5	0.5	3.9	6.7	0.2	4.6
5.0	175.8	30.2	10.5	0.8	6.4	11.0	0.4	7.6	112.9	20.8	6.7	0.6	4.2	7.4	0.3	5.1
5.2	181.4	32.7	10.9	1.0	6.7	12.1	0.5	8.3	114.7	22.3	6.9	0.8	4.3	8.0	0.4	5.6
5.4	185.3	35.2	11.3	1.2	7.0	12.9	0.7	8.9	115.8	23.4	7.0	0.9	4.4	8.6	0.5	5.8
5.6	188.7	36.8	11.5	1.4	7.2	13.7	0.8	9.5	116.6	24.4	7.0	1.1	4.4	9.0	0.7	6.1
5.8	190.9	38.5	11.7	1.6	7.4	14.4	1.1	9.8	116.5	25.0	7.0	1.3	4.4	9.2	0.8	6.2
6.0	192.4	39.9	11.8	1.9	7.4	14.9	1.3	10.2	115.8	25.8	6.9	1.3	4.5	9.4	1.0	6.3

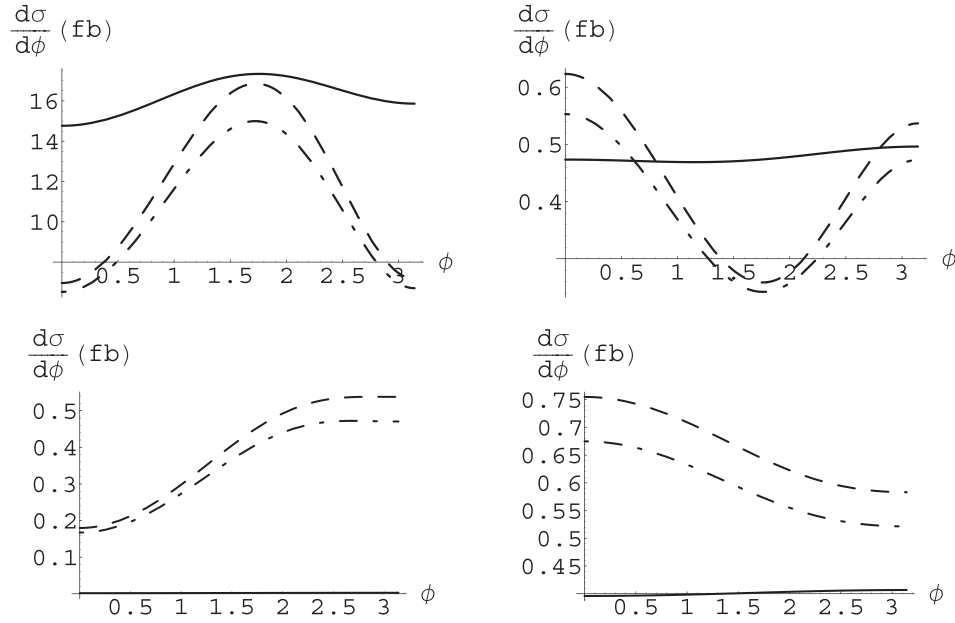


FIG. 3. The distributions of the relative angle ϕ between the electron and positron. (a), (b), (c), and (d) correspond to the distributions for η_c , χ_{c0} , χ_{c1} , χ_{c2} in the three detectors, respectively. Here $\theta_{\text{cut}} = \eta_{\text{cut}} = 20^\circ$. In each figure, the solid line, the dashed line, and the dot-dashed line represent the results from the BES-III, Belle, and BABAR, respectively.

Now, we proceed to study the distributions of the relative angle ϕ between the electron and positron for various charmonium production. In Fig. 3, we plot the distributions for η_c , χ_{c0} , χ_{c1} , χ_{c2} at tree level in the three detectors (we take the c.m. energy $\sqrt{s} = 3.78$ GeV at the BEPC-II),

where the azimuth angle cutoffs are taken as $\theta_{\text{cut}} = \eta_{\text{cut}} = 20^\circ$. In the figure, the solid line, the dashed line, and the dot-dashed line denote the results from the BES-III, Belle, BABAR, respectively. The distributions for the highly excited charmonia are not displayed, since their

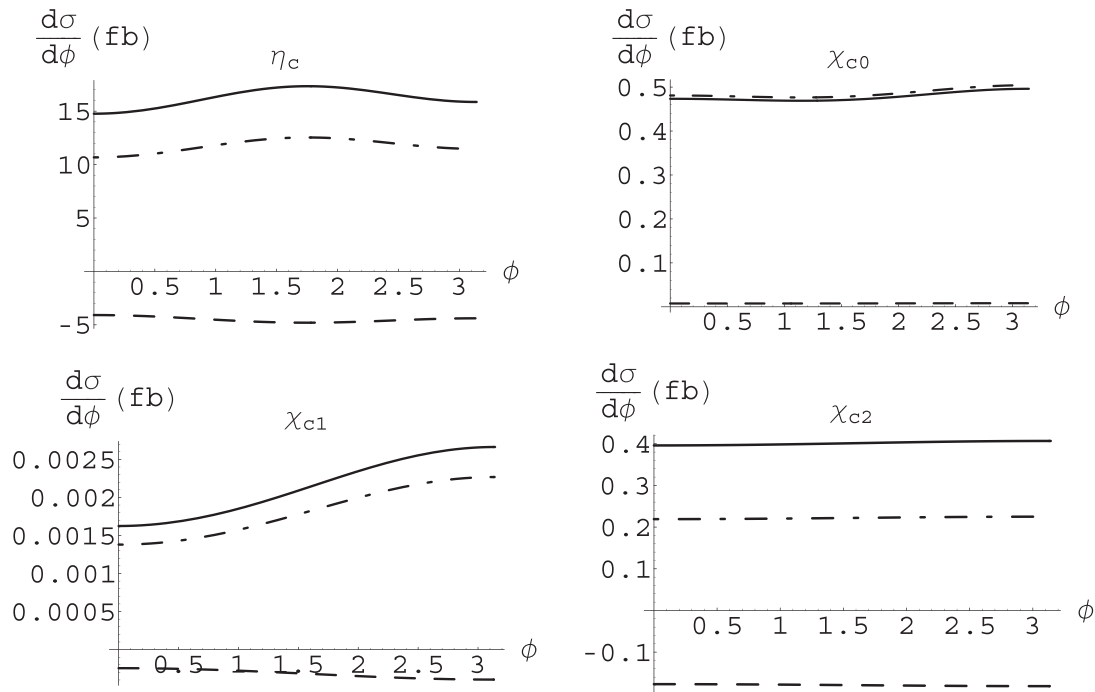


FIG. 4. The NLO radiative corrections to the distributions of relative angle ϕ for η_c , χ_{c0} , χ_{c1} , χ_{c2} at the BES-III ($\sqrt{s} = 3.78$ GeV), where the solid line, the dashed line, and the dot-dashed line represent the results from the tree level, the NLO radiative corrections and the total results, respectively.

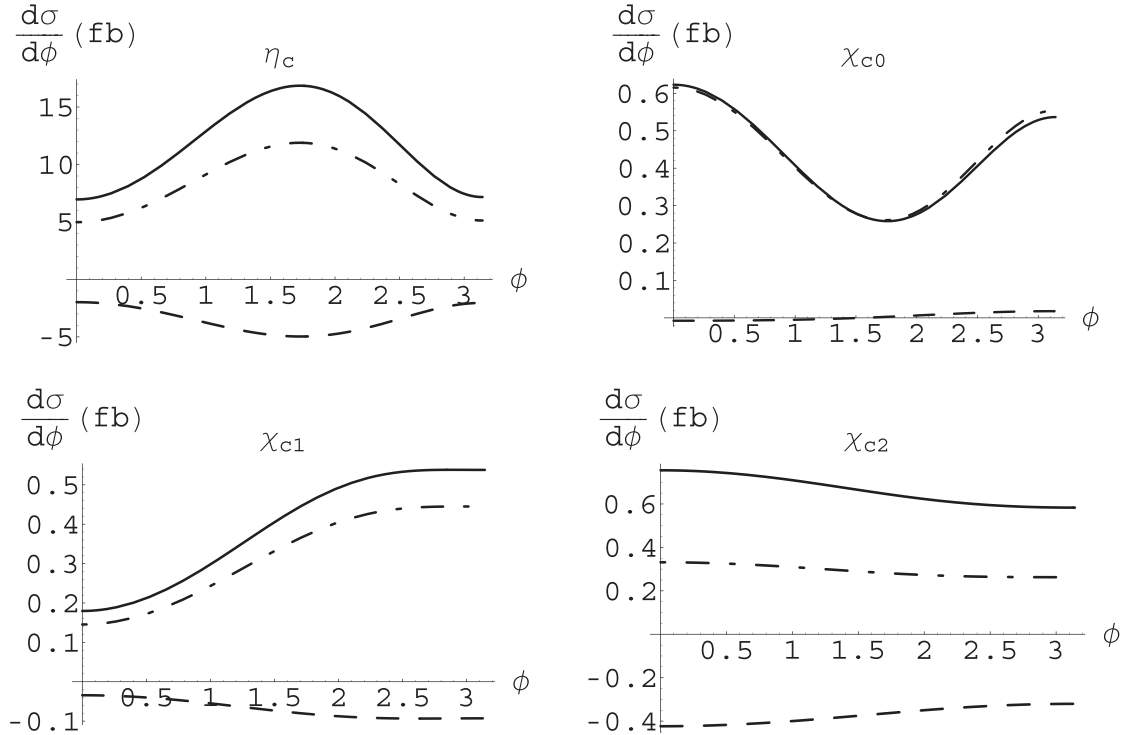


FIG. 5. The NLO radiative corrections to the distributions of relative angle ϕ for η_c , χ_{c0} , χ_{c1} , χ_{c2} at the Belle, where the solid line, the dashed line, and the dot-dashed line represent the results from the tree level, the NLO radiative corrections and the total results, respectively.

shapes are similar to these of the ground states. It is worthwhile to note that the angular distributions distinguish for different charmonia, therefore, as mentioned before, this feature can help experimenters to discriminate the hadrons.

Finally, we show the NLO radiative corrections to the distributions of the relative angle ϕ . Figures 4–6 illustrate the results at the BES-III, Belle, *BABAR*, respectively. From these figures, we noticed that the NLO radiative corrections only slightly modify the shapes of the distributions at tree level.

IV. SUMMARIES AND DISCUSSIONS

In the previous two sections, we calculated the cross sections for quarkonium production in the two-photon process up to the NLO QCD corrections. We propose that the quarkonia can be detected through measuring the emitted electron and positron. This indirect approach embraces two major benefits. One is that the emitted electron and positron are relatively easy to measure. The other is that the distribution of the relative angle between the electron and positron can be served as a sensitive probe to the quantum number of the quarkonium.

In Table I, we notice that the cross sections for bottomonium production in the two-photon process are tiny, compared with charmonium production. There are three primary causes responsible for the smallness. The first

is that the charge of the b quark is smaller than that of the c quark and the cross sections are proportional to e_Q^4 . One can find the second reason by noticing the squared amplitudes for S -wave quarkonium production are $|\mathcal{M}(S)|^2 \sim \frac{1}{m^4}$, while are $|\mathcal{M}(P)|^2 \sim \frac{1}{m^6}$ for P -wave quarkonium production, which can be seen from (13) or (14). Hence, the large b quark mass will suppress the cross sections for bottomonium production accordingly. The third reason originates from the phase-space integration, which is relatively large for charmonium production.

Prior to further discussion, we pause to roughly estimate the background mentioned in the introduction. As pointed out, the main background is $e^+e^- \rightarrow e^+e^-\gamma\gamma$, which may contaminate the signals in the peak of the charmonium mass. There are a total of forty Feynman diagrams for this process. Among them, the dominant contributions come from one kind of diagram, i.e., the final state's electron and positron separately emit one photon, which embraces several enhancements. In these diagrams, there are sizable collinear enhancements in the region where the electron and positron are collinear with photons. In addition, when the immediate virtual photon is soft, the cross section realizes a further linear enhancement. As a consequence, we are able to estimate the magnitude of the background by analyzing these diagrams. After some work, the cross section in the dominant region reduces to

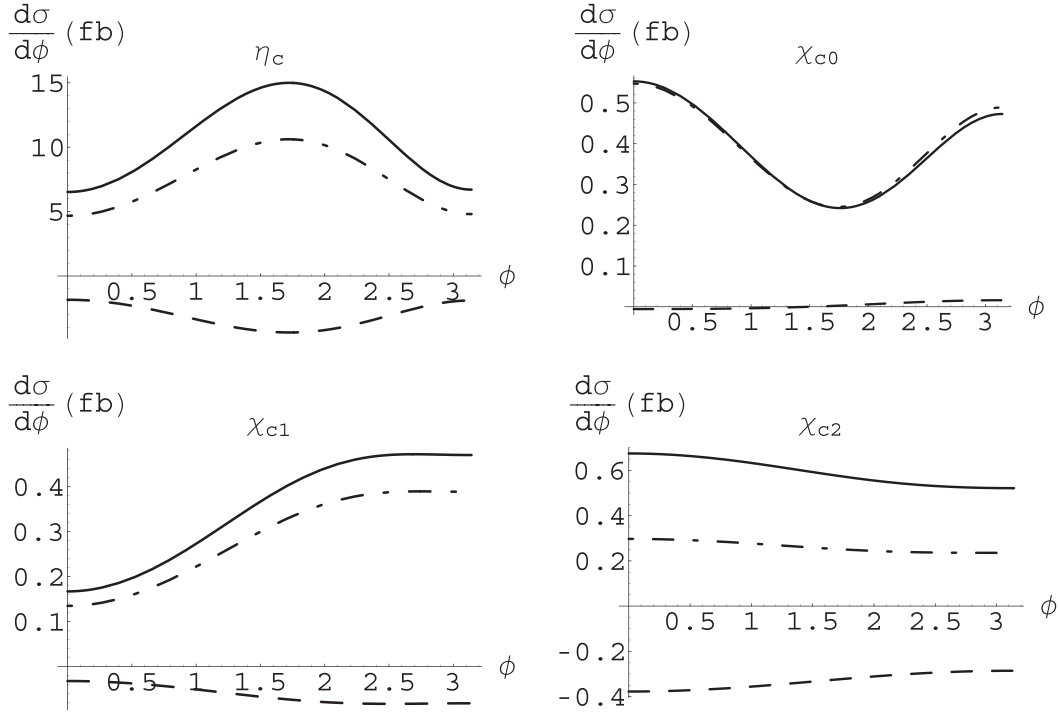


FIG. 6. The NLO radiative corrections to the distributions of relative angle ϕ for η_c , χ_{c0} , χ_{c1} , χ_{c2} at the *BABAR*, where the solid line, the dashed line, and the dot-dashed line represent the results from the tree level, the NLO radiative corrections and the total results, respectively.

$$\sigma \approx \frac{1}{2} \left(\frac{\alpha}{2\pi} \log \frac{s}{4m_e^2} \right)^2 \int \frac{dy}{y} \int \frac{dz}{z} [1 + (1-y)^2] \times [1 + (1-z)^2] \times \sigma(e^+e^- \rightarrow e^+e^-), \quad (25)$$

where $y = \frac{2E_1^0}{\sqrt{s}}$ and $z = \frac{2E_2^0}{\sqrt{s}}$ signify the energy fractions of the two photons.

In Eq. (25) we see the double logarithmic functions which correspond to the collinear divergences. The integration boundaries of the variables y, z are constrained by the condition that the invariable mass of the two photons locates in the neighbor of the charmonium mass:

$$\frac{4(m_H + \Gamma_H)^2}{s} \geq [(y+z)^2 - (y-z)^2] \geq \frac{4m_H^2}{s}, \quad (26)$$

where Γ_H denotes the decay width of the charmonium H . $\sigma(e^+e^- \rightarrow e^+e^-)$ is the cross section of the Bhabha scattering, where the t -channel is dominant

TABLE V. Cross sections (in units of fb) of background for charmonium H production. The azimuth angle between the final state's electron and positron is constrained to be $\theta' \leq 180^\circ - \theta_{\text{cut}}$, and we take $\theta_{\text{cut}} = 20^\circ$.

H	η_c	$\eta_c(2S)$	χ_{c0}	χ_{c1}	χ_{c2}	$\chi_{c0}(2P)$	$\chi_{c1}(2P)$	$\chi_{c2}(2P)$
BES-III	170	7	21	1	3
B -factories	250	54	63	5	11	110

$\sigma(e^+e^- \rightarrow e^+e^-) \approx \frac{8\pi\alpha^2}{s(1-\cos\theta_{\text{cut}})}$, where θ_{cut} corresponds to the cutoff for the angle between the initial electron and the emitted electron.

In the dominant region of the background, the final electron and positron are emitted back to back in the c.m. frame. By analyzing the signal process $e^+e^-e^+e^-H$, it is not hard to observe that only a small fraction of events is emitted in the opposite direction (the reason is that we have azimuth angular cutoffs for the emitted leptons). Therefore, we can go further to cut the background by setting a cutoff θ' (such as $\theta' \leq 180^\circ - \theta_{\text{cut}}$) for the azimuth angle between the final electron and positron. After this selection, we suppress one of the collinear enhancements from $\log \frac{s}{4m_e^2}$ to $\log(\frac{1}{\sin^2\theta_{\text{cut}}})$ for the background, however, we lose only a small fraction of the signal.

Now, we are able to estimate the cross sections of the background. By taking $\theta' \leq 180^\circ - \theta_{\text{cut}}$ and $\theta_{\text{cut}} = 20^\circ$, we get the corresponding cross sections of the background for various charmonium production, which are listed in Table V. Compared with Tables II and III, we find the cross sections of the background are several times larger than the corresponding signals, especially for χ_{c0} and $\chi_{c2}(2P)$. Nevertheless, the distributions of invariable masses of the two photons near the charmonium masses are rather flat for the background. This feature is distinctly different with the signals. We still expect the signals can be reconstructed in experiment, especially

TABLE VI. The event numbers (in units of/year) of charmonium production at the BES-III and B factories. The cutoffs are taken as $\theta_{\text{cut}} = \eta_{\text{cut}} = 20^\circ$.

	η_c	$\eta_c(2S)$	χ_{c0}	χ_{c1}	χ_{c2}	$\chi_{c0}(2P)$	$\chi_{c1}(2P)$	$\chi_{c2}(2P)$
BES-III	742	35	30	0.1	14
Belle	5380	1740	260	210	190	500	270	320
BABAR	4870	1560	240	180	170	450	240	290

for the channels whose background cross sections are only two or three times larger.

From Tables II and III, we explore and summarize the main conclusions:

- (1) The NLO radiative corrections are rather small for the χ_{c0} , while big for the χ_{c2} . This sharp contrast looks strange at first sight, however, it is reasonable by noticing that the NLO radiative corrections in the processes $H \rightarrow \gamma\gamma$ [7] are

$$\begin{aligned}
& \frac{\sigma_{\text{NLO}}(\eta_c \rightarrow \gamma\gamma) - \sigma_{\text{LO}}(\eta_c \rightarrow \gamma\gamma)}{\sigma_{\text{LO}}(\eta_c \rightarrow \gamma\gamma)} \\
&= \frac{\alpha_s}{\pi} C_F \left(-5 + \frac{\pi^2}{4} \right) \approx -28\%, \\
& \frac{\sigma_{\text{NLO}}(\chi_{c0} \rightarrow \gamma\gamma) - \sigma_{\text{LO}}(\chi_{c0} \rightarrow \gamma\gamma)}{\sigma_{\text{LO}}(\chi_{c0} \rightarrow \gamma\gamma)} \\
&= \frac{\alpha_s}{\pi} C_F \left(-\frac{7}{3} + \frac{\pi^2}{4} \right) \approx -1\%, \\
& \frac{\sigma_{\text{NLO}}(\chi_{c2} \rightarrow \gamma\gamma) - \sigma_{\text{LO}}(\chi_{c2} \rightarrow \gamma\gamma)}{\sigma_{\text{LO}}(\chi_{c2} \rightarrow \gamma\gamma)} \\
&= \frac{\alpha_s}{\pi} C_F (-4) \approx -44\%.
\end{aligned} \tag{27}$$

After checking the results in Tables II and III, we find the NLO radiative corrections in the two-photon process approximately agree with these in $H \rightarrow \gamma\gamma$ (except for the χ_{c1}). χ_{c1} decays into two on-shell photons is forbidden by the Yang theory, however, we can still make analysis by using the formulas of the radiative corrections to $\chi_{c1} \rightarrow \gamma\gamma^*$ in Ref. [11]. Concretely, in the limit of the virtual photon nearly on-shell, we find the radiative corrections are around -15% , which roughly agrees with the radiative corrections to the two-photon process in the two tables. Furthermore, for most of the cases, the NLO radiative corrections in the tables eventually deviate from the values given in (27) with the cutoffs increasing. This is due to the EPA.

- (2) The cross sections decrease quickly as the cutoffs increase. It is not surprising since the bulk of events concentrates on the direction of the beam. For this reason, the cutoffs for the detectors have a significant influence on the event numbers.

- (3) At the BES-III, the cross section for the χ_{c1} production is much smaller than those of others. It can be explained as that since the main contribution of the cross section comes from the region of the two virtual photons nearly on-shell, where the squared amplitude for the subprocess $\gamma\gamma \rightarrow H$ vanishes according to (16), due to the Yang theory. On the contrary, at the B factories, the cross sections of χ_{c1} are unexpectedly large and even greater than those of $\chi_{c0,2}$ for relatively large cutoffs. These relatively large cross sections are good news from the experimental perspective.

- (4) Taking into account the luminosity of the colliders, we are able to estimate the event numbers for charmonium production. The luminosity is $L \sim 1 \times 10^{33} \text{ cm}^{-2} \text{ s}^{-1}$ at the BEPC-II, and $L \sim 1 \times 10^{34} \text{ cm}^{-2} \text{ s}^{-1}$ at the KEKB and PEP-II. Thus, the event numbers are $N \sim L \times t \times \sigma \sim 1 \times 10^{33} \text{ cm}^{-2} \text{ s}^{-1} \times 10^7 \text{ s} \times \sigma = 10/\text{fb} \times \sigma$ at the BES-III, and $N \sim 10^2/\text{fb} \times \sigma$ at the B factories. Now, taking the cutoffs $\theta_{\text{cut}} = \eta_{\text{cut}} = 20^\circ$, and c.m. energy $\sqrt{s} = 3.78 \text{ GeV}$ at the BEPC-II, we give Table VI to show the event numbers of various charmonia in the three detectors. From the table, we find that all the event numbers are considerable at the B factories, as a result, we expect that they can be detected by observing the emitted electrons and positrons. The event number for the η_c at the BES-III is also large, so it should be detected, while the event numbers for the $\eta_c(2S)$, $\chi_{c0,2}$ are relatively moderate, it may be hard to be measured at the BES-III except there are more accumulations. The event number of the χ_{c1} is so small at the BES-III that it cannot be probed.

From Figs. 4–6, we find that the QCD radiative corrections only slightly modify the shapes of the distributions of the relative angle ϕ . Since the distributions are quite different for the charmonia with different quantum numbers, they can be used to determine the quantum numbers of the charmonia. Furthermore, we expect that the distribution may be used to search for the new particles. Since $X(3940)$ [22], $X(4160)$ [23], and $Z(3930)$ [24] are assumed to be the candidates of ordinary charmonia [25], experiments can confirm or deny these assumptions through observing the distribution of the relative angle ϕ .

ACKNOWLEDGMENTS

We thank Prof. Zhao-Xi Chang for discussions and suggestions. W.S. thanks Dr. Tamal K. Mukherjee for discussions. The research of W.S. was supported by China Postdoctoral Science Foundation under Grants No. 10875130 and No. 10935012. The research of Y.G. and Y.C. was supported by the NSFC with Contract No. 10875156.

- [1] N. Brambilla *et al.* (Quarkonium Working Group Collaboration), [arXiv:hep-ph/0412158](#); S. Uehara *et al.* (VENUS Collaboration), *Phys. Lett. B* **266**, 188 (1991); *Z. Phys. C* **63**, 213 (1994); T. Barnes, T. E. Browder, and S. F. Tuan, *Phys. Lett. B* **385**, 391 (1996); S. J. Brodsky, [arXiv:hep-ph/0010176](#); C. E. Carlson and M. Vanderhaeghen, *Annu. Rev. Nucl. Part. Sci.* **57**, 171 (2007); H. Nakazawa (Belle Collaboration), *Nucl. Phys. B, Proc. Suppl.* **184**, 220 (2008).
- [2] J. J. Aubert *et al.* (E598 Collaboration), *Phys. Rev. Lett.* **33**, 1404 (1974); J. E. Augustin *et al.* (SLAC-SP-017 Collaboration), *Phys. Rev. Lett.* **33**, 1406 (1974).
- [3] C. Amsler *et al.* (Particle Data Group Collaboration), *Phys. Lett. B* **667**, 1 (2008); K. Nakamura *et al.* (Particle Data Group Collaboration), *J. Phys. G* **37**, 075021 (2010).
- [4] V. M. Budnev, I. F. Ginzburg, G. V. Meledin, and V. G. Serbo, *Phys. Rep.* **15**, 181 (1975); S. J. Brodsky, T. Kinoshita, and H. Terazawa, *Phys. Rev. Lett.* **25**, 972 (1970).
- [5] G. T. Bodwin, E. Braaten, and G. P. Lepage, *Phys. Rev. D* **51**, 1125 (1995); **55**, 5853(E) (1997).
- [6] G. T. Bodwin and A. Petrelli, *Phys. Rev. D* **66**, 094011 (2002).
- [7] A. Petrelli, M. Cacciari, M. Greco, F. Maltoni, and M. L. Mangano, *Nucl. Phys.* **B514**, 245 (1998).
- [8] E. Braaten and J. Lee, *Phys. Rev. D* **67**, 054007 (2003); **72**, 099901(E) (2005).
- [9] M. E. Peskin and D. V. Schroeder, *An Introduction To Quantum Field Theory* (Westview Press, Boulder, CO, 1995).
- [10] E. Braaten and Y.-Q. Chen, *Phys. Rev. D* **57**, 4236 (1998); **59**, 079901(E) (1999).
- [11] W.-L. Sang and Y.-Q. Chen, *Phys. Rev. D* **81**, 034028 (2010).
- [12] D. Li, Z.-G. He, and K.-T. Chao, *Phys. Rev. D* **80**, 114014 (2009).
- [13] R. Mertig, M. Bohm, and A. Denner, *Comput. Phys. Commun.* **64**, 345 (1991).
- [14] E. J. Eichten, K. Lane, and C. Quigg, *Phys. Rev. D* **69**, 094019 (2004).
- [15] G. T. Bodwin, J. Lee, and C. Yu, *Phys. Rev. D* **77**, 094018 (2008).
- [16] H.-K. Guo, Y.-Q. Ma, and K.-T. Chao, *Phys. Rev. D* **83**, 114038 (2011).
- [17] H. S. Chung, J. Lee, and C. Yu, *Phys. Rev. D* **78**, 074022 (2008).
- [18] G. T. Bodwin, H. S. Chung, D. Kang, J. Lee, and C. Yu, *Phys. Rev. D* **77**, 094017 (2008).
- [19] G. T. Bodwin, D. Kang, and J. Lee, *Phys. Rev. D* **74**, 014014 (2006).
- [20] G. T. Bodwin, E. Braaten, D. Kang, and J. Lee, *Phys. Rev. D* **76**, 054001 (2007).
- [21] E. J. Eichten and C. Quigg, *Phys. Rev. D* **52**, 1726 (1995).
- [22] K. Abe *et al.* (Belle Collaboration), *Phys. Rev. Lett.* **98**, 082001 (2007).
- [23] P. Pakhlov *et al.* (Belle Collaboration), *Phys. Rev. Lett.* **100**, 202001 (2008).
- [24] S. Uehara *et al.* (Belle Collaboration), *Phys. Rev. Lett.* **96**, 082003 (2006).
- [25] R. Chistov, *Nucl. Phys. B, Proc. Suppl.* **185**, 146 (2008).